Three-body calculation of incoherent π^0 photoproduction on a deuteron

A. Fix[1,*] and H. Arenhövel[2,†]
[1]*Tomsk Polytechnic University, 534050 Tomsk, Russia*
[2]*Institut für Kernphysik, Johannes Gutenberg-Universität Mainz, 55099 Mainz, Germany*

(Received 10 April 2019; revised manuscript received 19 August 2019; published 25 September 2019)

Incoherent π^0 photoproduction on a deuteron in the $\Delta(1232)$ region is treated in a three-body scattering approach using separable two-body interactions. Results are presented for total and differential cross sections. It turns out that the role of higher order terms beyond the first order in the multiple scattering series is insignificant, and their inclusion cannot explain the existing discrepancy between theory and experiment.

DOI: 10.1103/PhysRevC.100.034003

I. INTRODUCTION

The role of the final state interaction (FSI) in incoherent π^0 photoproduction on a deuteron

$$\gamma + d \to \pi^0 + n + p \tag{1}$$

has been studied by various groups [1–6]. In general, the theoretical treatment of this reaction was based on the multiple scattering picture, in which, however, only the first order terms with respect to the final NN and πN interactions are taken into account. According to these studies, the main FSI effect arises from NN rescattering, whereas the contribution from πN rescattering is rather small.

It is well known that in the reaction in Eq. (1) the first-order inclusion of the NN interaction has a particularly strong effect compared to the impulse approximation (IA). The reason for this feature is the fact that in contrast to processes with charged pions, $\gamma d \to \pi^+ nn/\pi^- pp$, for the incoherent π^0 production (1) the impulse approximation contains a spurious contribution of the coherent reaction ($\gamma d \to \pi^0 d$) since the final plane wave is not orthogonal to the deuteron ground state [3,7,8]. Indeed, projecting out the ground state from the final plane wave, the so-called modified IA, comprises already the dominant part of the first order FSI correction [3]. The remaining FSI effect is of the same order as for charged pion production. Further incorporation of πN rescattering gives an additional (however much less significant) decrease. Thus the total first-order FSI effect in the Δ-resonance region is a decrease of the total cross section by about 30% compared to the one predicted by the pure spectator model (IA).

On the other hand, the calculation including only the first order rescattering terms still overestimates the experimental total cross section [9,10] by about 15% at the $\Delta(1232)$ peak. It appears reasonable to assume that the remaining difference could be assigned to the neglect of the higher order terms, which can cause an additional broadening of the Δ resonance and, consequently, can lead to a lowering of the Δ peak in the cross section.

In the present work we study the role of the higher orders of the multiple scattering series in the reaction (1). To this end, we calculate the reaction amplitude using the three-body scattering theory. In the next section we briefly outline the formalism. Our approach is based on a separable representation of the driving two-body πN and NN interactions. As is well known, in this case the original three-body equations simplify to a set of equations of Lippman-Schwinger type for a system of coupled quasi-two-body channels. To reduce this set into an easily solvable one-dimensional form, we apply an expansion into partial waves. In Sec. III we present our results and compare them with existing experimental data. We also discuss the importance of the multiple scattering corrections. Conclusions are given in the final section (Sec. IV).

II. FORMALISM

In the present approach we use for the description of the final $\pi^0 np$ three-body state two coupled two-body channels, each consisting of a quasiparticle formed by two of the three particles and the remaining one as a spectator. Thus each quasiparticle is an interacting two-body system. The two channels are in detail:

(i) Channel "d" consisting of a deuteron as a quasiparticle with two interacting nucleons and a pion as spectator.
(ii) Channel "Δ" consisting of an interacting nucleon-pion system forming a Δ as quasiparticle and a spectator nucleon.

In the following we use $\alpha, \beta, \ldots \in \{d, \Delta\}$ to label the channels and the corresponding quasiparticles, while $a, b, \ldots$ are used for the corresponding spectators. In this notation the channel α consists of a spectator a and two interacting particles (bc) forming the quasiparticle α.

Treating the electromagnetic interaction perturbatively in lowest order one obtains for the reaction T matrix

$$T = \sum_{\alpha \in \{d,\Delta\}} X^\alpha \, \tau_\alpha g_\alpha \,, \tag{2}$$

*fix@tpu.ru
†arenhoev@uni-mainz.de

FIG. 1. Diagrammatic representation of the T matrix in Eq. (2).

where X^α denotes a channel amplitude, τ_α the channel propagator, and g_α the quasiparticle vertex for $(bc) \to b + c$. A graphical representation of the T matrix in terms of the channel amplitudes is shown in Fig. 1.

The amplitudes X^α obey a set of coupled equations, which can be derived from the Faddeev three-body formalism under the assumption of separable two-body interactions. In operator form they read

$$X^\alpha = \sum_{\beta\in\{d,\Delta\}} X^\beta \, \tau_\beta \, Z^{\beta,\alpha} + Z^{\gamma d,\alpha}, \quad \alpha \in \{d, \Delta\}. \tag{3}$$

These equations are shown in a graphical representation in Fig. 2.

The driving terms $Z^{\alpha,\beta}$ describe the exchange of a particle c between the quasiparticles α and β. The term $Z^{\gamma d,\Delta}$, forming the inhomogeneous part of the set (3), contains the electromagnetic vertex $\gamma N \to \Delta$. Obviously one has $Z^{\gamma d,d} = 0$.

In momentum space the potentials $Z^{\alpha,\beta}$ have the following form:

$$Z^{\alpha,\beta}(\vec{p}_a, \vec{p}_b; W) = \frac{g_\alpha(q_\alpha) g_\beta(q_\beta)}{W - E_a(p_a) - E_b(p_b) - E_c(|\vec{p}_a + \vec{p}_b|) + i\epsilon}. \tag{4}$$

Here, W denotes the total energy in the center-of-mass (c.m.) frame, $\vec{p}_a$ and $\vec{p}_b$ the c.m. momenta of the spectator particles of the channels α and β, respectively. The relative momenta $\vec{q}_{\alpha/\beta}$ between the spectators of the channels β/α, respectively, and the exchanged particle in the arguments of the vertices $g_{\alpha/\beta}(q_{\alpha/\beta})$ are treated nonrelativistically, e.g.,

$$\vec{q}_\alpha = \vec{p}_b + \frac{M_b}{M_b + M_c} \vec{p}_a \tag{5}$$

with M_c denoting the mass of the exchanged particle, whereas for the particle energies we use the relativistic relation $E_a(p) = \sqrt{p^2 + M_a^2}$.

To reduce Eq. (3) to a numerically manageable form we exploit a partial wave expansion of the amplitudes X^α in terms of the total angular momentum J and the isospin T. We use the LS coupling scheme by coupling the total angular momentum $\vec{j}_\alpha$ of the quasiparticle with the spin $\vec{s}_a$ of the third particle to the total channel spin $\vec{S}_\alpha$. The orbital momentum $\vec{L}_\alpha$ is then coupled with $\vec{S}_\alpha$ to the total angular momentum $\vec{J}$. For the

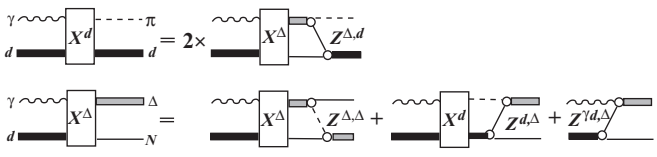

FIG. 2. Diagrammatic representation of the system of three-body equations of Eq. (3). The factor 2 in the first equation arises from the symmetrization of the two nucleons.

given values of photon polarization $\vec{\epsilon}_\lambda$, initial deuteron spin projection M_d, total spin S_α with projection M_{S_α}, and total isospin T of the final quasi-two-body state α the partial wave expansion of the channel amplitudes $X^{\alpha,T}_{\lambda M_d S_\alpha M_{S_\alpha}}(\vec{k}, \vec{p}; W)$ reads

$$X^{\alpha,T}_{\lambda M_d S_\alpha M_{S_\alpha}}(k, \vec{p}; W) = \frac{N_d}{\sqrt{4\pi}} \sum_{J^\pi} \sum_{L,S,M_S} \sqrt{2L+1} \sum_{L_\alpha, M_\alpha} X^{\alpha,T;J^\pi}_{LS,L_\alpha S_\alpha}(k, p; W) \, Y^*_{L_\alpha M_\alpha}(\hat{p}) \times (1\lambda \, 1M_d | SM_S)(L0 \, SM_S | JM_S)(L_\alpha M_\alpha \, S_\alpha M_{S_\alpha} | JM_S), \tag{6}$$

where the factor N_d takes into account the deuteron normalization. In Eq. (6) the z axis is chosen along the initial photon momentum $\vec{k}$.

With the help of this partial wave decomposition one obtains from Eq. (3) a set of one-dimensional coupled equations for each value of J, parity π, and isospin T in the following form (for simplicity we drop the energy W in the arguments):

$$X^{\alpha,T;J^\pi}_{LS,L_\alpha S_\alpha}(k, p) = Z^{\gamma d,\alpha,T;J^\pi}_{LS,L_\alpha S_\alpha}(k, p) + \sum_{\beta\in\{d,\Delta\}} \sum_{L_\beta,S_\beta} \int \frac{p'^2 dp'}{(2\pi)^3} \times X^{\beta,T;J^\pi}_{LS,L_\beta S_\beta}(k, p') \, \tau_\beta(w_\beta(p')) Z^{\beta,\alpha,T;J^\pi}_{L_\beta S_\beta, L_\alpha S_\alpha}(p', p), \tag{7}$$

where $\alpha \in \{d, \Delta\}$, and k denotes the momentum of the incident photon. The argument w_β of the propagator τ_β is the quasiparticle energy calculated on the assumption that the corresponding spectator b is on-shell:

$$w^2_\beta(p') = W^2 - 2W E_b(p') + M_b^2 \tag{8}$$

with $E_b(p') = \sqrt{p'^2 + M_b^2}$. The spin S of the initial γd state in Eq. (7) is a vector sum of the deuteron spin $\vec{s}_d$ and the photon circular polarization vector $\vec{\epsilon}_\lambda$ with components $(\vec{\epsilon}_\lambda)_\mu = -\delta_{-\mu\lambda}$. The partial wave components of the driving terms $Z^{\beta,\alpha,T;J^\pi}_{L_\beta S_\beta, L_\alpha S_\alpha}$ are obtained using the formalism developed, e.g., in Ref. [11].

In the present calculation we have included states with total angular momentum up to $J_{\max} = 7$ of both parities with a maximum orbital momentum $L_{\max} = 9$. Furthermore, since the dominating Δ resonance term only enters states with total isospin $T = 1$, we neglect contributions of the $T = 0$ part. Therefore, we omit in the subsequent equations the isospin notation. As a result, for each total spin and parity J^π we have at most six coupled one-dimensional integral equations, two equations for the channel $\alpha = d$ and four for $\alpha = \Delta$.

Our basic ingredient is a separable representation of the scattering amplitudes in the πN and NN two-body subsystems. For $\pi N \to \Delta \to \pi N$ we take

$$t_\Delta(\vec{q}, \vec{q}'; z) = g^\dagger_\Delta(\vec{q}) \, \tau_\Delta(z) \, g_\Delta(\vec{q}') \tag{9}$$

with

$$\tau_\Delta(z) = \frac{1}{z - M^0_\Delta - \Sigma_\Delta(z)}, \tag{10}$$

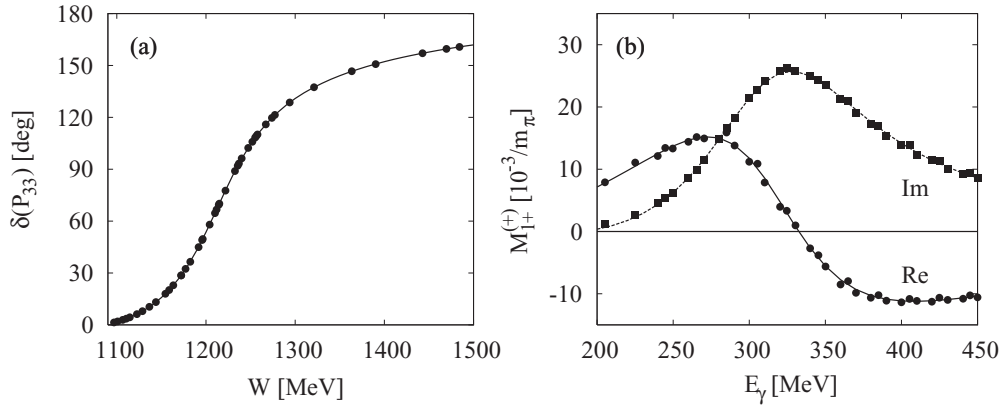

FIG. 3. (a) Present fit to the P_{33} πN phase shifts using Eqs. (9)–(12). The data are taken from the compilation in Ref. [12]. (b) The $M_{1+}^{(+)}$ multipole for $\gamma N \to \pi N$. Solid and dashed curves are fit for real and imaginary parts, respectively. The full circles and squares show the energy independent multipole analysis from Refs. [13,14].

where M_Δ^0 denotes the bare Δ mass, and

$$\Sigma_\Delta(z) = \frac{1}{4}\sum_{m,m_\Delta}\int \frac{d^3q}{(2\pi)^3}\,\frac{\left|\left\langle \tfrac{1}{2}\,m\middle|g_\Delta(\vec{q}\,)\middle|\tfrac{3}{2}\,m_\Delta\right\rangle\right|^2}{z - E_\pi(q) - E_N(q) + i\epsilon} \tag{11}$$

the $\Delta \to \pi N$ self-energy.

The vertex g_Δ is taken in the standard form (the isospin part is omitted) with a monopole form factor

$$g_\Delta(\vec{q}\,) = \frac{f_{\pi N\Delta}}{m_\pi}\,(\vec{\sigma}_{\Delta N}\cdot\vec{q}\,)\,\frac{\beta_\Delta^2}{\beta_\Delta^2 + q^2}\sqrt{\frac{M_N}{2E_\pi(q)E_N(q)}}\,, \tag{12}$$

where m_π denotes the pion mass and $\vec{\sigma}_{\Delta N}$ the $N \to \Delta$ spin transition operator. The parameters M_Δ^0, $f_{\pi N\Delta}$, and β_Δ were adjusted to the πN phase shifts in the P_{33} channel. The resulting fit, presented in panel (a) of Fig. 3, gives $M_\Delta^0 =$ 1306 MeV, $f_{\pi N\Delta}^2/4\pi = 0.8113$, and $\beta_\Delta = 295$ MeV.

For the electromagnetic transition $\gamma N \to \Delta$ only the dominant $M1$ part is taken into account. The corresponding vertex function was parametrized in the form

$$g_\Delta^\gamma(z,\vec{k}\,) = e\frac{G^{M1}(z)}{2M_N}(\vec{\sigma}_{\Delta N}\cdot(\vec{k}\times\vec{\epsilon}_\lambda)) \tag{13}$$

with e for the elementary charge, and the magnetic transition moment

$$G^{M1}(z) = \mu_\Delta(z)\,e^{i\Phi_\Delta(z)} \tag{14}$$

with modulus $\mu_\Delta(z)$ and phase $\Phi_\Delta(z)$.

The off shell-behavior of the vertex (13) is determined by the analytic continuation of the transition moment $G^{M1}(z)$ of Eq. (14) into the complex plane of z. Below the single-nucleon threshold we use

$$G^{M1}(z) = G^{M1}(m_\pi + M_N)\,, \tag{15}$$

for $\Re\, z < m_\pi + M_N$. The approximation (15) obviously violates analyticity of the amplitude. However, as the direct calculation shows, the subthreshold region provides only a small fraction of the resulting cross section, at least in the energy region not very close to the threshold, so that this shortcoming of our model does not visibly affect the results.

Following Ref. [15] we fit the energy dependence of $\mu_\Delta(z)$ and $\Phi_\Delta(z)$ in such a way that the resulting $\gamma N \to \Delta \to \pi N$ amplitude

$$t_\Delta^\gamma(\vec{k},\vec{q};z) = g_\Delta^\dagger(\vec{q}\,)\,\tau_\Delta(z)\,g_\Delta^\gamma(z,\vec{k}\,) \tag{16}$$

reproduces the isovector magnetic amplitude $M_{1+}^{(+)}$ in the energy region from threshold up to 450 MeV [panel (b) in Fig. 3]. Thus, we do not treat the background terms (crossed nucleon pole and ω exchange) exactly, but their contribution is effectively included via adjustment of the ansatz in Eqs. (13)–(16) to the data of $M_{1+}^{(+)}$. The magnitude $\mu_\Delta(z)$ and the phase $\Phi_\Delta(z)$ in Eq. (14) are parametrized as

$$\mu_\Delta(z) = \sum_{n=0}^{4} C_n\left(\frac{z}{M_\Delta}\right)^n, \quad \Phi_\Delta(z) = \sum_{n=0}^{4} D_n\left(\frac{z}{M_\Delta}\right)^n \tag{17}$$

with $M_\Delta = 1232$ MeV. The constants C_n and D_n resulting from the fit in Fig. 3 are collected in Table I.

In the NN sector only the s waves $^3S_1$ and $^1S_0$ are taken into account, neglecting the contribution of the tensor component $^3D_1$. For the s-wave interactions we use the rank-one separable parametrization of the Paris potential from Ref. [16]:

$$v_d^{(s)}(\vec{q},\vec{q}\,') = -g_d^{(s)}(q)\,g_d^{(s)}(q'\,) \tag{18}$$

with

$$g_d^{(s)}(q) = (2\pi)^{3/2}\sum_{n=1}^{6}\frac{C_n^{(s)}}{q^2 + \left(\beta_n^{(s)}\right)^2}, \tag{19}$$

where the index s refers to singlet or triplet states. The parameters $C_n^{(s)}$ and $\beta_n^{(s)}$ are listed in [16].

The coupled integral equations in Eq. (7) were solved using the matrix inversion method. To overcome the problem of

TABLE I. Listing of constants C_n and D_n of the parametrizations in Eq. (17).

n	0	1	2	3	4
C_n	37.848	−29.789	−19.951	12.261	4.4393
D_n	−12.901	19.163	4.4974	−14.938	4.2943

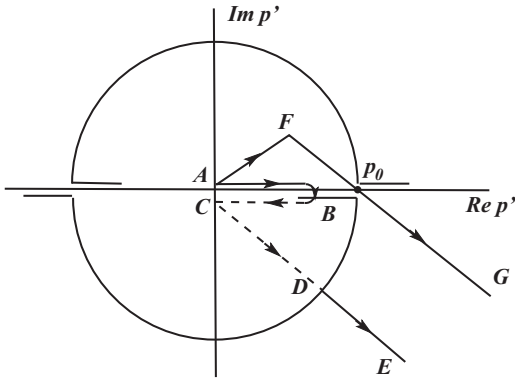

FIG. 4. Integration contours and configuration of the cuts in the complex p' plane. The dashed line shows the part of the contour on the second sheet.

singularities we used the well known procedure in which the integration contour is shifted from the real axes to the fourth quadrant of the complex p' plane. This technique is quite well known (e.g., see Ref. [17]), and there is no need to describe it here in detail. Some formal aspects related to the relativistic kinematics were considered in Ref. [18].

Here, we would like to comment only on some details concerning the treatment of the singularities of the driving terms $Z^{\beta,\alpha,T;J^\pi}_{L_\beta S_\beta, L_\alpha S_\alpha}$ having the configuration shown in Fig. 4. It is known that in order to find the X^α matrix at real momenta, one has to perform a continuation of the driving terms $Z^{\beta,\alpha,T;J^\pi}_{L_\beta S_\beta, L_\alpha S_\alpha}$ in Eq. (7) onto the second Riemann sheet (the part BCD of the integration contour in Fig. 4). However, in this case the driving term $Z^{\beta,\alpha,T;J^\pi}_{L_\beta S_\beta, L_\alpha S_\alpha}(p', p)$ behaves near $p' = 0$ as $(1/p')^{L+1}$. As a result the integrand in Eq. (7) strongly diverges at the origin and one finds large contributions near the point C. However, the resulting large contributions coming from the intervals BC and CD essentially cancel each other thus leading to a significant loss of numerical accuracy via a small difference of two large numbers. This problem was also mentioned in Ref. [19], where the break-up reaction $nd \to nnp$ was studied. In Ref. [19] the three-body equations were solved only for low values of L ($L \leqslant 3$), whereas for higher L only the first order approximation or the inhomogeneous term was considered.

In the present case, we use another integration contour (the polygonal curve AFG in Fig. 4). The driving terms are always calculated on the first Riemann sheet, and the integration does not pose any numerical problem. A certain disadvantage of this method lies in the fact that the position of the momentum p_0, where the contour is squeezed between the logarithmic cuts (see Fig. 4), depends on the value of the on-shell momentum p in Eq. (7). For this reason one has to solve the set of Eq. (7) separately for each value of p of the chosen mesh.

After inversion of the system in Eq. (7) and the determination of the partial wave amplitudes $X^{\alpha,T;J^\pi}_{LS,L_\alpha S_\alpha}(k, p; W)$, one obtains the corresponding channel amplitudes $X^\alpha_{\lambda M_d\, S_\alpha M_{S_\alpha}}(\vec{k}, \vec{p}; W)$ from Eq. (6), from which, finally, the reaction amplitude $T_{\lambda M_d\, m_1 m_2}$ [see Eq. (2)] as function of the momenta of the final particles $\vec{q}_\pi$, $\vec{p}_1$, and $\vec{p}_2$ follows

$$
\begin{aligned}
&T_{\lambda M_d\, m_1 m_2}(k, \vec{p}_1, \vec{p}_2, \vec{q}_\pi) \\
&\quad = \sum_{M'_d} X^d_{\lambda M_d\, 1 M'_d}(k, \vec{q}_\pi; W) \left(\frac{1}{2} m_1 \frac{1}{2} m_2 \middle| 1 M'_d\right) \tau^{(1)}_d(w_d(q_\pi))\, g^{(1)}_d(q_{NN}) \\
&\quad + \left[\sum_{m_\Delta} \sum_{S_\Delta, M_\Delta} \sqrt{\frac{2}{3}}\, X^\Delta_{\lambda M_d\, S_\Delta M_\Delta}(k, \vec{p}_1; W) \left(\frac{1}{2} m_2 \frac{3}{2} m_\Delta \middle| S_\Delta M_\Delta\right) \tau_\Delta(w_\Delta(p_1)) \left\langle \frac{3}{2} m_\Delta \middle| g_\Delta(\vec{q}_{\pi N_2}) \middle| \frac{1}{2} m_1 \right\rangle - (1 \leftrightarrow 2) \right]. \qquad (20)
\end{aligned}
$$

Here, the vector $q_{\pi N_i}$, $i = 1, 2$, denotes the relative momentum in the subsystem πN_i, and q_{NN} the relative momentum of the two final nucleons. As is mentioned above, in the present calculation we took into account only configurations with total isospin $T = 1$, since those with $T = 0$ do not contain the dominant $N\Delta$ configuration. Therefore, in the first term on the right-hand side of Eq. (20) only the two-nucleon states with total spin $S_d = 1$ contribute.

Using the amplitude of Eq. (20), the fully exclusive differential cross section for the present reaction in the overall center-of-mass frame is given in terms of the T matrix [Eq. (20)]

$$
\begin{aligned}
\frac{d\sigma}{dq_\pi\, d\Omega_\pi\, d\Omega^*_{NN}} &= \frac{1}{(2\pi)^5} \frac{E_d\, E_p\, E_n\, q_\pi^2\, p^*_{NN}}{2W \omega_\gamma\, \omega_{NN}} \frac{1}{6} \\
&\quad \times \sum_{\lambda, M_d, m_1, m_2} \left| T_{\lambda M_d\, m_1 m_2}(k, \vec{p}_1, \vec{p}_2, \vec{q}_\pi) \right|^2, \qquad (21)
\end{aligned}
$$

where E_d, E_p, E_n, and ω_γ denote the total energies of the corresponding particles, and ω_{NN} the invariant NN energy. The nucleon momentum in the np center-of-mass system is denoted by p^*_{NN} and its spherical angle by Ω^*_{NN}.

III. RESULTS AND DISCUSSION

Before applying the formalism to incoherent pion photoproduction, we first test our model by considering the inelastic scattering of pions on a deuteron. The corresponding equations are obtained from Eq. (3) by the replacement of the driving term according to $Z^{\gamma d,\Delta} \to Z^{\pi d,\Delta}$. The method of inversion of the corresponding three-particle equations remains of course the same.

The results are presented in Fig. 5. As already noted in [20], the significant influence of the final state interaction on the magnitude and shape of the differential cross section is due to the orthogonality of the wave functions of the initial and the

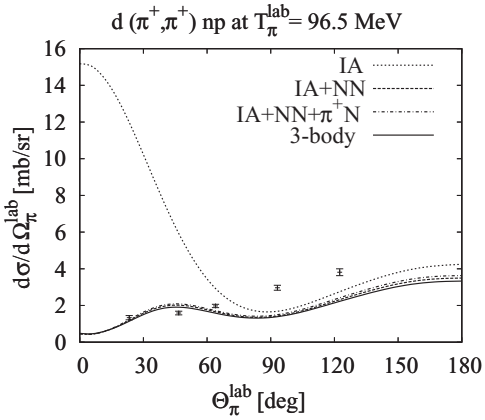

FIG. 5. Differential cross section of the reaction $\pi^+ d \to \pi^+ np$ for an incident pion laboratory kinetic energy of 96.5 MeV. The dotted curve is the result of the impulse approximation (IA). Dashed and dash-dotted curves are obtained with first order np and in addition $\pi^+ N$ rescattering contributions. Solid curve: three-body calculation. The data are from Ref. [21].

final np states. In particular, this effect leads to a substantial suppression of the plane wave cross section (I A) at forward angles, and, as a result, to a general agreement with the data [21] in the forward direction.

In the region around $\theta_{\rm lab} = 90^\circ$ our cross section underestimates the experimental results and turns out to be lower than the theoretical cross section obtained in Ref. [20]. The latter deviation is apparently caused by a disagreement seen already between the IA results. Namely, our plane wave cross section is almost twice as small in this region as that obtained in [20]. At the same time, the FSI effects predicted by our model and in Ref. [20] are in reasonable agreement.

As the analysis of the curves in Fig. 5 shows, the FSI effect is almost completely reproduced by including only the first-order rescattering contributions. In particular, this concerns the np interaction whereas pion rescattering gives only a small addition at the level of 0.5–1 %. Inclusion of the remaining higher order terms within the three-particle model does not lead to any noticeable change in the cross section in the entire range of pion angles. Since the dynamics of the process $\gamma d \to \pi^0 np$ associated with FSI is essentially similar to that of the inelastic $\pi^+ d$ scattering, it is reasonable to expect that qualitatively the same picture will be observed in the incoherent pion photoproduction.

Turning now to the reaction $\gamma d \to \pi^0 np$ we start the discussion by considering the role of different partial waves in the total cross section as is shown in Fig. 6 for the IA [panel (a)] and the full three-body calculation [panel (b)]. Similar to the coherent photoproduction $\gamma d \to \pi^0 d$ [22] the largest contribution in the incoherent reaction comes from the 2^+ wave, which predominantly is an $M1$ transition, leading to the production of pions with angular momentum $l_\pi = 1$ with respect to the np system. This partial wave alone contributes almost 45% to the total IA cross section in the Δ region. The next important partial waves are 2^- and 3^- generating basically pions with $l_\pi = 2$. The other partial waves give much smaller contributions to the total cross section.

Inclusion of FSI [see panel (b) of Fig. 6] leads to a visible decrease of $\sigma(2^+)$ by a factor of 2–3, whereas $\sigma(3^-)$ (predominantly $M2$) is considerably enhanced and becomes even slightly larger than $\sigma(2^+)$. Next in importance is $\sigma(2^-)$, which is also increased by FSI by about 10%. The contributions of the higher partial waves is still quite insignificant. Most of the FSI effects are already contained in the first order rescattering contribution except for the dominant 2^+-partial wave as is demonstrated in Fig. 7 where the higher orders still give a significant contribution. It is worth noting that the state 2^+ corresponds to the s-wave ΔN configuration $^5S_2$. In this respect, the importance of three-body effects in this wave agrees with our naive expectation that the absence of the centrifugal barrier in the $^5S_2$ state leads to a significant overlap of the potentials in all three two-body subsystems.

As already mentioned, the corresponding partial wave series was cut off at $J_{\rm max} = 7$ and $L_{\rm max} = 9$. In order to demonstrate the good convergence for this value of $J_{\rm max}$ we show in Fig. 8 the semiexclusive differential cross section with respect to the final pion as function of a few lower $J_{\rm max}$ values. Similar to the results for the elastic pion-deuteron scattering of

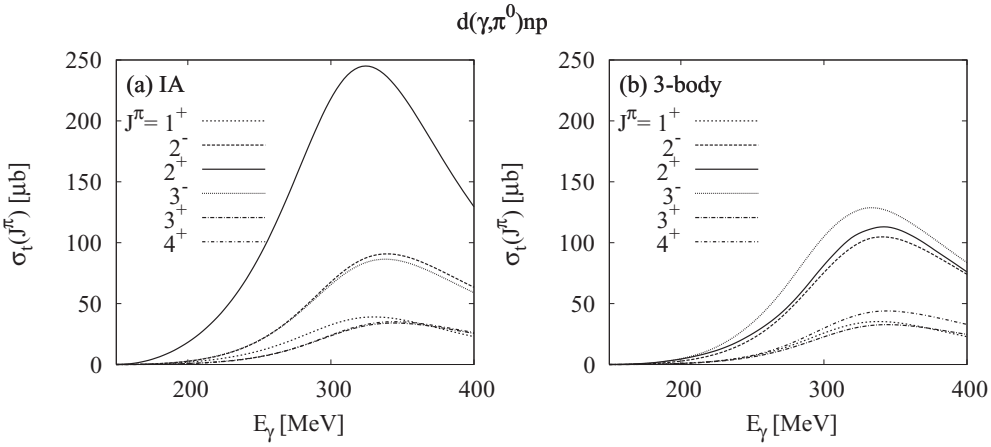

FIG. 6. Contributions of various partial waves J^π to the total cross section $\gamma d \to \pi^0 np$: (a) impulse approximation: (b) three-body calculation.

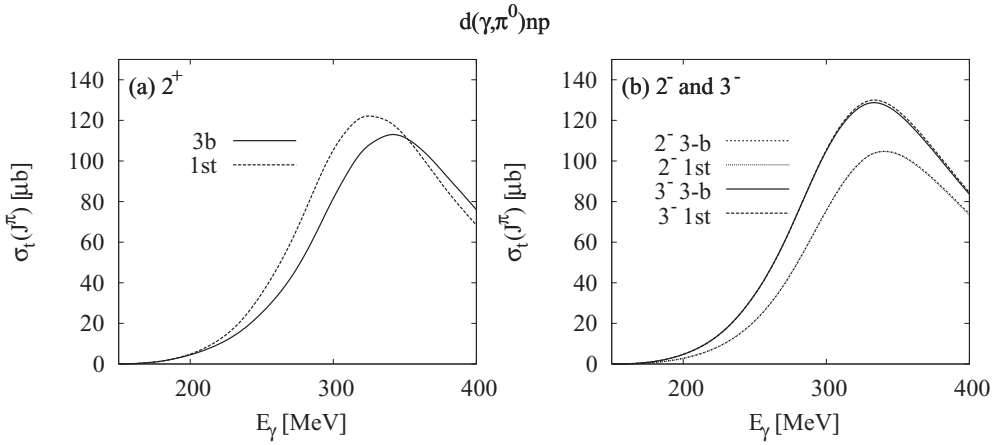

FIG. 7. Comparison of the first order rescattering calculation (1st) with the three-body one (3-b) for the most important partial waves: (a) 2^+; (b) 2^- and 3^-.

Ref. [23], this approximation provides a satisfactory convergence in the Δ-resonance region as one can see: changing $J_{\max}$ from 5 to 7 has already quite a small effect, so that the choice $J_{\max} = 7$ appears to be acceptable.

In Fig. 9 we show in panel (a) the total cross section as function of the incident photon energy and in panel (b) the differential cross section at $E_\gamma = 330$ MeV, calculated in the present three-body model. These results can be compared with our previous calculation in Ref. [3]. In the latter case the single nucleon amplitude $t(\gamma N \to \pi N)$ was taken from the MAID analysis [24] and the inclusion of FSI was reduced to the first order contributions (i.e., to np and πN rescatterings in the final state). The present result, which is obtained in a somewhat oversimplified model for $\gamma N \to \pi N$ (pure resonance ansatz for the $M_{1+}^{(+)}$ multipole, and neglect of the tensor component of the deuteron wave function) agrees quite well with those of Ref. [3]. Figure 9 clearly shows that the multiple scattering corrections do not visibly change the reaction dynamics. Inclusion of only the first order corrections, i.e., np and πN rescatterings in the final state, turns out to be sufficient.

In the same Fig. 9 [panel (a)] we compare our results with experimental total cross section data from Ref. [9]. Whereas

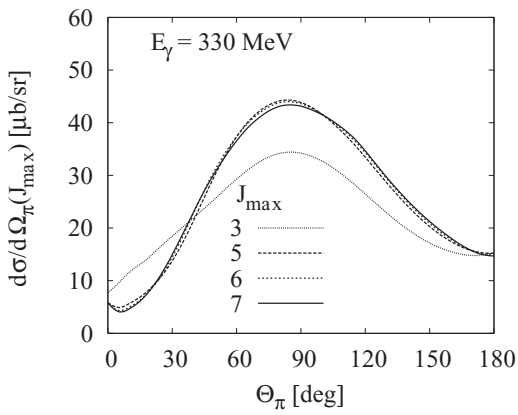

FIG. 8. Differential cross section $\gamma d \to \pi^0 np$ in the center-of-mass frame at $E_\gamma = 330$ MeV for various values of the maximum total angular momentum $J_{\max}$ of the partial wave expansion.

in the region below the $\Delta(1232)$ peak the agreement is satisfactory, the theory is too high in the region near the maximum ($E_\gamma \gtrsim 300$ MeV). This discrepancy was already discussed in Refs. [2–4]. In particular it was conjectured in [3] that the difference may come from the neglect of the ΔN interaction which might lead to a broadening of the Δ resonance due to additional inelasticities. The present calculation, which effectively takes into account the ΔN interaction, shows, that this effect is negligible in the incoherent reaction and cannot explain the discrepancy.

There is still the unresolved question about the importance of true pion absorption, which is not taken into account by the present model. We however assume that its role in our reaction is not significant for the following reasons. Firstly, the two-nucleon absorption of pions is effective only in the region of small internucleon distances, which are not important in the breakup process. Secondly, the calculations performed by us in the framework of the so-called bound state picture (BSP), in which one of the nucleons is represented as a bound πN state with the quantum numbers P_{11} [25], give a correction to the total cross section of only about 0.5%. It is worth noting, that the BSP-based approach is not entirely correct, since in fact it treats the nucleons in the intermediate NN states as distinguishable particles, and today various sophisticated methods have been developed to incorporate the NN channel into the three-particle πNN equations. However, one can hardly expect that even a correct treatment of the NN states will dramatically increase their role in our reaction. Our assumption about the insignificance of true pion absorption is also in accord with the results of Ref. [26] where a similar conclusion was reached for the πd inelastic scattering.

IV. CONCLUSION

In this paper we have presented a calculation of total and differential cross sections for the incoherent reaction $\gamma d \to \pi^0 np$ in the energy region from threshold up to the Δ resonance. The calculation is based on a three-body model for the inclusion of the final πNN interaction. Although we use some simplifications (nonrelativistic three-body equations, neglect of the deuteron d wave), the most significant features of the

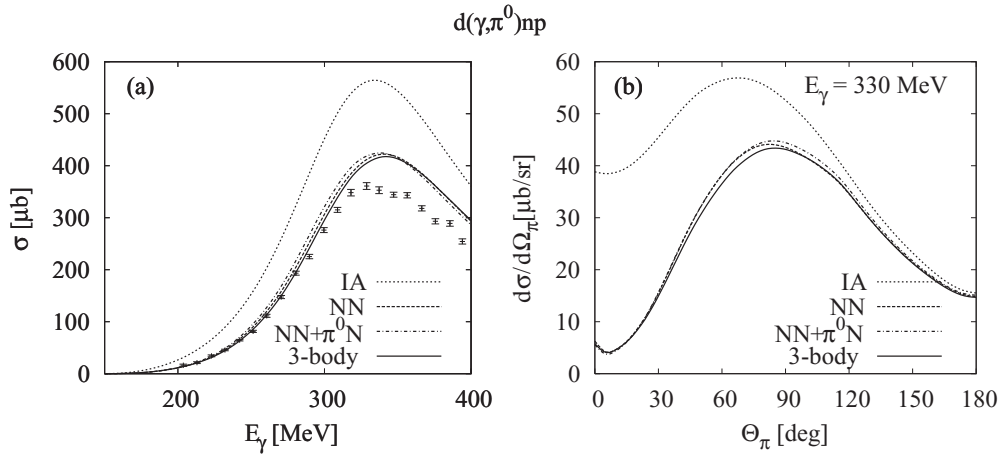

FIG. 9. Total (a) and differential (b) cross sections of the reaction $\gamma d \to \pi^0 np$. Dotted curves: impulse approximation (IA) (the inhomogeneous $Z^{\gamma d,\alpha}$ terms in Fig. 2). Dashed and dash-dot curves include first order np and in addition $\pi^0 N$ rescattering contributions, respectively. Solid curves: full three-body calculation. The data are from Ref. [9].

process are preserved, including the importance of the $M1$ multipole transition $\gamma N \to \Delta$ and the dominance of the Δ resonance in πN scattering.

The results show that the corrections due to multiple scattering are quite insignificant in the major part of the kinematical region. As already mentioned in the introduction, the major importance of FSI in the $\pi^0 np$ channel is related to the orthogonality of the initial and the final np wave functions. This effect is taken into account essentially already by the first order FSI contributions as can be seen from the fact that inclusion of the np rescattering (dashed curve on the right panel of Fig. 9) leads to a significant decrease of the differential cross section at very forward pion angles, that is, in the region where the momentum transferred to the nucleon system is minimal.

According to our results, the full three-body calculation changes the cross section compared to the first-order rescatterings only by about 1–2 % in the Δ resonance region. Since the multiple scattering corrections are insignificant their inclusion cannot explain the existing deviation between the theoretical and experimental results. The theory still visibly overestimates the data, as is shown in panel (a) of Fig. 9. The problem concerning the difficulties in describing the photoproduction of π^0 on a deuteron in the first resonance region was also addressed in Ref. [10]. In this work the authors had analysed the inclusive cross section $\gamma d \to \pi^0 X$ with X being either a deuteron or a neutron-proton scattering state.

As is shown in Ref. [27] using the closure approximation for the final two-nucleon state, the sum of both cross sections should be equal to the sum of the free-nucleon cross sections, folded with the nucleon momentum distribution in a deuteron. The latter is approximately equal to the cross section $\sigma_{\rm IA}$ of $\sigma(\gamma d \to \pi^0 np)$ calculated in the spectator model. However, as the calculation in Ref. [10] shows, $\sigma_{\rm IA}$ overestimates by about 15% the experimental total cross section for $\gamma d \to \pi^0 X$. Since the free proton cross section is well known the natural conclusion would be that the free neutron cross section is overestimated by the existing multipole analyses (in Ref. [10] the MAID [24] and SAID [28] analyses are considered). In order to bring the theory into agreement with the data of [9,10] the theoretical neutron cross section has to be decreased by about 25%. Such a strong isospin dependence of the elementary amplitude can hardly be explained within the existing models for $\gamma N \to \pi N$. According to these models the reaction is strongly dominated by the $\Delta(1232)$ resonance so that the proton and neutron cross sections are nearly equal. Thus the question about the source of the discrepancy between theoretical predictions and data in the $\Delta(1232)$ region remains open.

ACKNOWLEDGMENTS

This work was supported by the Deutsche Forschungsgemeinschaft (Collaborative Research Center 1044). A.F. acknowledges additional support from the Tomsk Polytechnic University Competitiveness Enhancement Program.

[1] J. M. Laget, Phys. Rep. **69**, 1 (1981).
[2] E. M. Darwish, H. Arenhövel, and M. Schwamb, Eur. Phys. J. A **16**, 111 (2003).
[3] A. Fix and H. Arenhövel, Phys. Rev. C **72**, 064005 (2005).
[4] M. I. Levchuk, A. Y. Loginov, A. A. Sidorov, V. N. Stibunov, and M. Schumacher, Phys. Rev. C **74**, 014004 (2006).
[5] V. E. Tarasov, W. J. Briscoe, M. Dieterle, B. Krusche, A. E. Kudryavtsev, M. Ostrick, and I. I. Strakovsky, Phys. At. Nucl. **79**, 216 (2016).
[6] S. X. Nakamura, Phys. Rev. C **98**, 042201(R) (2018).
[7] J. V. Noble, Phys. Rev. C **17**, 2151 (1978).
[8] F. Cannata, J. P. Dedonder, and L. Lesniak, Phys. Rev. C **33**, 1888 (1986).

[9] B. Krusche *et al.*, Eur. Phys. J. A **6**, 309 (1999).
[10] U. Siodlaczek *et al.*, Eur. Phys. J. A **10**, 365 (2001).
[11] M. Stingl and A. S. Rinat (Reiner), Nucl. Phys. A **154**, 613 (1970).
[12] G. Rowe, M. Salomon, and R. H. Landau, Phys. Rev. C **18**, 584 (1978).
[13] F. A. Berends and A. Donnachie, Nucl. Phys. B **84**, 342 (1975).
[14] R. A. Arndt, R. L. Workman, Zhujun Li, and L. D. Roper, Phys. Rev. C **42**, 1853 (1990).
[15] P. Wilhelm and H. Arenhövel, Nucl. Phys. A **609**, 469 (1996).
[16] H. Zankel, W. Plessas, and J. Haidenbauer, Phys. Rev. C **28**, 538 (1983).
[17] R. Aaron and R. D. Amado, Phys. Rev. **150**, 857 (1966).
[18] A. Fix and H. Arenhövel, Nucl. Phys. A **697**, 277 (2002).
[19] R. T. Cahill and I. H. Sloan, Nucl. Phys. A **165**, 161 (1971); **196**, 632(E) (1972).
[20] H. Garcilazo, Phys. Rev. C **47**, 957 (1993).
[21] M. A. Khandaker, M. Doss, I. Halpern, T. Murakami, D. W. Storm, D. R. Tieger, and W. J. Burger, Phys. Rev. C **44**, 24 (1991).
[22] P. Wilhelm and H. Arenhövel, Nucl. Phys. A **593**, 435 (1995).
[23] A. S. Rinat and A. W. Thomas, Nucl. Phys. A **282**, 365 (1977).
[24] D. Drechsel, O. Hanstein, S. S. Kamalov, and L. Tiator, MAID: available at http://www.kph.uni-mainz.de/
[25] R. Aaron, R. D. Amado, and J. E. Young, Phys. Rev. **174**, 2022 (1968).
[26] H. Garcilazo, Phys. Rev. Lett. **53**, 652 (1984).
[27] V. M. Kolybasov and V. G. Ksenzov, Sov. J. Nucl. Phys. **22**, 372 (1976).
[28] R. A. Arndt *et al.*, SAID: available at http://gwdac.phys.gwu.edu/.